Innovative Graphene-PDMS Sensors for Aerospace Applications

Filomena Piscitelli*[1], Gennaro Rollo[2], Fabio Scherillo[3], Marino Lavorgna[2]

[1]*CIRA - Italian Aerospace Research Centre, via Maiorise, Capua, 81043, Italy*
[2]*Institute for Polymers, Composites and Biomaterials, National Research Council, Portici, 80055, Italy*
[3]*Department of Chemical, Materials and Production Engineering of the University of Naples Federico II, 8012, Naples, Italy*

*Corresponding author: E-mail: f.piscitelli@cira.it

Received: 19 October 2018, Revised: 17 December 2018 and Accepted: 19 December 2018

DOI: 10.5185/amlett.2019.0003
www.vbripress.com/aml

Abstract

For aerospace morphing and deployable applications, the use of PDMS-based sensors is crucial because they are characterized by easy application on large surfaces, light design, very large deformations, and durability in harsh environmental conditions. In this contest, the goal of the present work is to manufacture innovative, highly deformable, piezoresistive sensors, manufactured by using a simplified and scalable method for the applications on large-area, such as the airplane wings. To this end, an ad-hoc polymeric matrix was designed by crosslinking Polydimethylsiloxane (PDMS) oligomers OH terminated with siloxane domains, obtained from hydrolysis and condensation of tetraethyl orthosilicate (TEOS). In particular, the solution of siloxanes domains precursors contributes to lower the viscosity without any solvents and to create, after curing, a fine crosslinked system which could withstand high deformation. Nanocomposites with graphene (6 ÷ 15 wt%) were prepared by dispersing the filler into the polymeric precursor by adopting both magnetic stirring and sonication. Regardless the dispersion method and the filler concentration, few-layers of graphene coexists with large aggregations, and the electrical conductivity and the Gauge Factor increase as the graphene content increases. It was found that the graphene filler tends to hinder the evaporation of solvents developed during the crosslinking reactions, generating porosity and enhancing conductivity. A better filler dispersion obtained through sonication reduces the conductivity. All nanocomposites show a good linear relationship between the strain and the relative electrical resistance change, since the non-linearity remains below the 5%, and quite no-drift can be observed in a wide operative range.

Keywords: Graphene, PDMS, piezoresistive sensors, stretchable electronics.

Introduction

In the next future, aerospace structural systems will incorporate distributed sensor networks for implementing several concepts ranging from health structure monitoring, including self-sensing properties for auto-inspection, to deployable and morphing components integrated with supervising active control systems [**1-4**]. In this view, there is a high demand of technological developments in the field of innovative materials, which can be used as sensors. Cheapness, ease of installation, lightness and wide deformation range are among the main key properties this kind of devices should have. These challenging targets may be well addressed by the innovative piezoresistive materials, which should then be integrated in responsive sensor networks. Non-conventional properties are requested, including the capability of undergoing large deformations (around 5%), [**5, 6**], and durability into harsh environmental conditions (temperature range -50 ÷ 80 °C, RH up to 100%, severe pressure excursions and many other aspects) [**7**]. In order to fulfil these designing requisites and overcome the difficulties linked with the large number of needed elements, lightweight piezo-resistive materials, sprayed directly on the surfaces of the structural systems to be observed and capable of experiencing very large deformation without affecting their usability appear as an extremely promising solution. Such a target may be achieved by exploiting the concepts of graphene-based elastomeric nanocomposites by tailoring the hierarchical distribution as well as the filler-filler and filler-polymer interaction of graphene platelets within the polymeric phase. Most of the recent literature is focused on these issues [**8, 9**], and several and various solutions were proposed. Some researcher employed CVD for the manufacturing of such a sensor, which in general show high sensitivity and reliability. For instance, Zhao *et al.* [**10**] developed a sensor having high sensitivity with a Gauge Factor (GF) over 300, and high deformability by using the plasma-enhanced CVD method. Whereas Yong *et al.* [**11**] achieved strain up to 100% using CVD–graphene growth

film onto plastic substrate. However, the high production costs, and complex processes of CVD methods hinder the development of any technological solution toward practical applications. Alternately, melt-mixing as well as solution processing addressed to realize graphene-based composite is expected to provide a low-cost and scalable method for the production of strain sensors. Yan *et al.* [**12**], for instance, reported on freestanding and flexible papers composed of crumpled graphene and nanocellulose produced by vacuum filtration. The resulting graphene-based paper was embedded in a stretchable elastomer PDMS to fabricate the strain sensor with improved stretchability from 6% (graphene paper) to 100% (graphene paper/PDMS). Alternatively, Kim *et al.* [**13**] achieved strain of 30% by using pre-strained graphene film and PDMS. However, all mentioned manufacturing methods could not match the requirement of cheap, sprayable and simplified process. In this respect, Hempel *et al.* [**14**] manufactured thin films of overlapping graphene flakes by using the spray coating method for highly tunable Gauge Factor strain sensors. This concept has proven to be a cheap, controlled, and useful for the film deposition on a wide variety of substrates. However, the authors employed 1-methylpyrrolidone (NMP) to disperse the graphene, compromising safety applications directly on the substrate (e.g., an aircraft component, for the aerospace applications). Also Bu *et al.* [**15**] prepared highly stretchable PDMS-based films by spray coating. They employed high temperatures to remove solvents and cure the silicone rubber matrix, and had the necessity to rinse the sensors in order to remove sodium dodecyl sulfate (SDS) useful to disperse the graphene. Therefore, to the best of our knowledge, highly stretchable sensors manufactured by using low-cost, sprayable, environmentally friendly, and scalable method for the production and the in-situ application of large-area ultrathin graphene films are still not present in literature. In this contest, the goal of the present work was to design and manufacture with a simplified low-cost method, highly stretchable strain sensor, which can be deposited directly on the substrate by spraying coating. In particular, an ad-hoc polymeric matrix was designed and optimized to exhibit low viscosity before curing, without the use of solvents, high strain deformation, thermal stability in the temperature range of -50÷80 °C, and room temperature curing. The idea was to disperse the graphene filler directly into the low-viscosity polymeric matrix, realized by using commercial PDMS grade OH terminated at two different molecular weights, which was solubilized in presence of TEOS, as precursors of siloxane domains, without the use of any solvents. The strain sensors were then obtained by dispersing the graphene (6 ÷ 15 wt%) into the polymeric matrix by adopting two different approaches: magnetic stirring or sonication. The nanocomposites were characterized by Scanning and Transmission Electron Microscopy (SEM and TEM), Raman spectroscopy, and by electrical–mechanical testing, with the aim to correlate the graphene spatial distribution with the electrical behavior. It was found that regardless the filler concentration few-layer platelets always coexist with large aggregates whose content, as expected, increases as the concentration of graphene increases. In all nanocomposite samples, there is a good interaction between graphene platelets/aggregates and PDMS and no detachment can be observed. Although the spatial distribution of graphene seems not being significantly affected by the preparation method, i.e., stirring or sonication, the electrical resistance of nanocomposites changes markedly. The highest conductivity of the nanocomposites prepared by mechanical stirring could be ascribed to the formation of a percolated and interconnected three-dimensional network, which enhancing the contact among the graphene platelets/aggregates, promote the conductivity [**16-19**]. On the opposite, a more homogeneous filler dispersion, obtained in the sonicated samples, could be responsible of the reduced conductivity. Finally, the developed sensors exhibit a satisfying linear relationship between the applied strain and the relative electrical resistance variation, and no drift of resistance change can be observed in a wide operational range.

Experimental

Materials/ chemicals details

Polydimethylsiloxane (PDMS) OH-terminated, having two different molecular weight, i.e., Mw = 110000 and Mw = 550, Tetraethyl orthosilicate (TEOS) and Dibutyltin dilaurate (DBTDL), were purchased by Sigma Aldrich. The Graphene (G), supplied by Ad-Nano Technologies, has a surface area of 350 m^2/g, an average thickness (z) of 2÷4 nm, and an average lateral dimension (x & y) of 5÷10 μm.

Material synthesis

The polymeric matrix (F1) was prepared by mixing two OH-terminated PDMS having molecular weights of 110000 and 550, respectively, TEOS, and DBTDL at room temperature. Sol-gel reactions, namely the alcohol and water condensations, take place among the -OH of the PDMS and CH_3CH_2O-, or alternately the -OH of TEOS partially hydrolyzed by humidity, achieving the crosslinking of the elastomeric matrix (F1). The PDMS-Graphene (PDMS-G) nanocomposites were prepared by dispersing the Graphene powder (6 ÷ 15 wt%) into the polymeric matrix for 30 minutes by using magnetic stirring (samples labelled as "M") or for 2 hours by using sonication (A = 40%, 30s on and 30s off; samples are labelled as "S"). The strain sensors consist of an insulating mold, made of cured F1, in which the conductive PDMS-G dispersion was poured (see **Fig. 1**). This design allows to applying the strain sensors directly on metallic substrates avoiding electrical contact between the electrical sensor and the substrate.

Fig. 1. Schematic (a) and picture (b) of the PDMS-G strain sensor.

Characterizations / device fabrications / response measurements

Scanning Electron Microscopy (SEM) analyses was carried out by using an Inspect F model FEI apparatus at an accelerating voltage of 10 kV. Transmission electron microscopy (TEM) imaging was performed using a Tecnai G2 Spirit TWIN electron microscope (FEI) operating at 120 kV on TEM-foils obtained from the bulk samples using a ultramicrotome Leica EM UC7, cryo mode, at -140 °C, cut rate between 1 and 8 mm/s, nominal feed 140 nm. The mechanical tests were performed, according to the standard ISO 527-2 [20], at 1 mm/min with an Instron 5564, on samples of 50 mm long and 4 mm wide. The samples' thickness was measured in five points with a digital micrometer QUANTUMIKE IP-65. The Raman spectra were collected at room temperature with a microRaman spectrometer Renishaw operating with a 514 nm laser source. Coupled electrical–mechanical testing was applied to evaluate the sensing characteristics and piezoresistive behaviour of PDMS-G nanocomposites. The experimental setup-up consists of a mechanical tester (Instron 5564 Tensile & Compression Materials Testing Electromechanical Em Tester) and a multimeter (Agilent 34401A 6½ Digit Multimeter) controlled by a homemade LabVIEW program. The electrical resistance was monitored continuously while the samples were submitted out to a tensile deformation with a control of the strain between 0 and 5%, with a rate of 0.7 mm/min, at room temperature (25 °C). The multimeter was set up with the measurement 2-probe method.

Results and discussion

In **Fig. 2** the SEM images of F1-6G-M, F1-15G-M, F1-6G-S and F1-15G-S at 250, 1000 and 2000x of magnification, performed on the upper and the fracture surfaces, respectively, are reported. Strong interactions and no delamination effects at the PDMS-Graphene platelets/aggregates interfaces are evident (see the fracture surfaces in **Fig. 2**). At highest filler content, i.e., 15wt%, graphene tends to aggregate in flakes of several micron in dimensions, as evident especially in the F1-15G-S sample (**Fig. 2**). It also highlights that the evaporation of water and ethyl alcohol produced by the sol-gel reaction generates diffused porosity, observable in almost all the samples. Additional porosity can be observed especially in the upper side of the samples (**Fig. 2**). The formation of this porosity becomes more evident as the graphene content increases, as shown in **Fig. 2** for the F1-15G-M sample. This may be ascribed to the evaporation of the developed solvents, which could be very fast in the M samples, leaving porosity, and on the contrary, hindered in the S samples, due to the presence of few-layers particles, resulting more controlled and uniform.

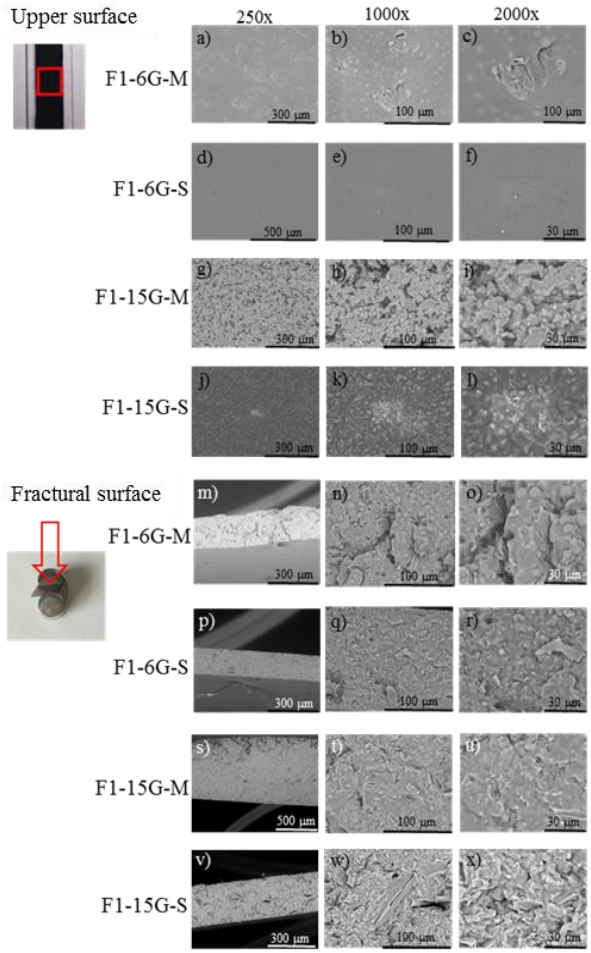

Fig. 2. SEM images performed on the upper surfaces (a-l), and on the fractural surfaces (m-x) of the F1-6G-M, F1-15G-M, F1-6G-S, and F1-15G-S samples. Left images are acquired at 250x, the central ones at 1000x, and the right images at 2000x.

TEM images (**Fig. 3**) performed on the F1-15G-M and F1-15G-S samples, give evidence of the presence of large aggregates of graphene together with few-layers for both samples. It is also worth noting that the polymeric matrix well adheres and penetrates the graphene flakes. Consequently, the Young's modulus of the nanocomposites increases, as reported in **Table 1**. Mechanical tests also highlight that the addition of the graphene nanoplatelets does not strongly affect the elastomeric properties of nanocomposites, since the corresponding elongation at break is reduced of only 5-10% with respect to the neat elastomeric matrix F1 (see values in **Table 1**).

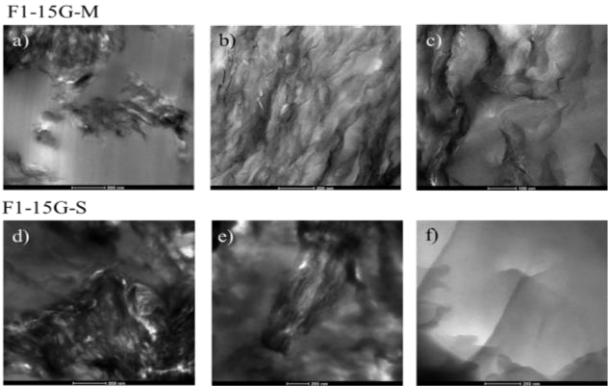

Fig. 3. TEM images of the F1-15G-M and F1-15G-S samples.

Table 1. Young's Modulus (E'), stress (σ_b) and strain at break (ε_b) of samples.

Sample	E'[MPa]	σ_b[MPa]	ε_b [%]
F1	5.0 ± 1.0	1.0 ± 0.2	19 ± 4
F1-6G-M	5.6 ± 0.3	1.4 ± 0.1	17 ± 2
F1-10G-M	7.7 ± 0.5	1.4 ± 0.1	17.1 ± 0.5
F1-15G-M	8.0 ± 1.0	1.5 ± 0.4	18 ± 2

Raman spectra were collected by sampling different, randomly selected, parts of the detected surfaces (some examples are reported in the insert of **Fig. 4**). It was found that, in spite of the graphene concentration and the preparation method, both the D band at 1350 cm^{-1} and G band at 1575 cm^{-1} are present. The presence of the D band, together with the blue-shift of the G band at 1595 cm^{-1}, can be attributed to the structural disorder of few-layers graphene nanoparticles which confirm their presence. The intensity ratio of D-band to G-band can be then used to measure the dispersion degree of graphene, since this ratio approaches zero for highly ordered pyrolytic graphite [**21, 22**]. This ratio was calculated by averaging on 10 different measures randomly performed on the samples' surface. In **Fig. 5**, it highlights that this ratio decreases as the graphene content increases, highlighting the aggregation of graphene at high content. These results confirm that regardless the dispersion method, by increasing the graphene content, the amount of graphene aggregation increases as well, and the effect of disorder, which can be attributed to the content of single or few-layers graphene nanoplateletes, decreases. Additionally, it highlights that at the same graphene content, the amount of few-layer nanoparticles present in sonicated samples is higher than that contained in the stirred samples (see **Fig. 5**)

Results of piezoresistive tests highlight that all samples exhibit a stable piezoresistive response with neglectable drift during the strain/unstrain cycles in a wide range of operational conditions. In **Fig. 6a**, changes in resistance are reported for the F1-15G-M sample, as an example. It also highlights that there is a right correspondence between the imposed strain and the measured electrical resistance change. In this regards, the best fit straight line of the measured experimental resistance was extrapolated with the aim to quantify the linearity in the piezoresistive response of the developed sensors.

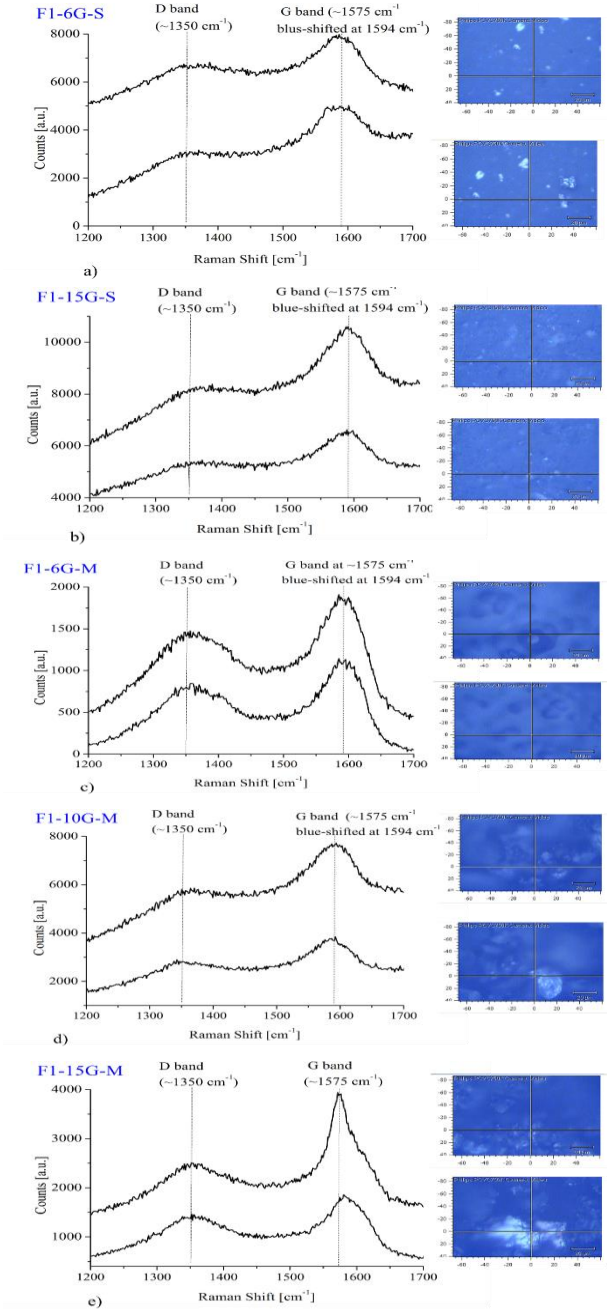

Fig. 4. Raman spectra of the F1-6G-S (a), F1-15G-S (b), F1-6G-M (c), F1-10G-M (d), and F1-15G-M (e) samples. On the inserts, the optical images of the tested points.

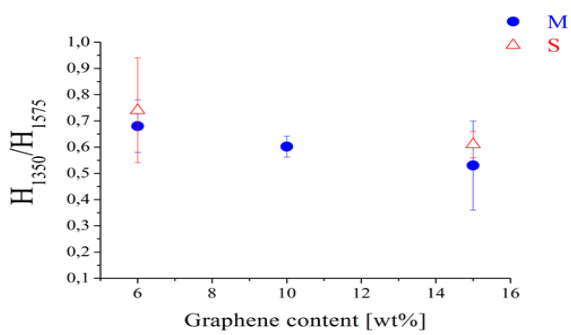

Fig. 5. Intensity ratio of D-band at 1350 cm^{-1} to G-band at 1575cm^{-1} as function of the graphene content.

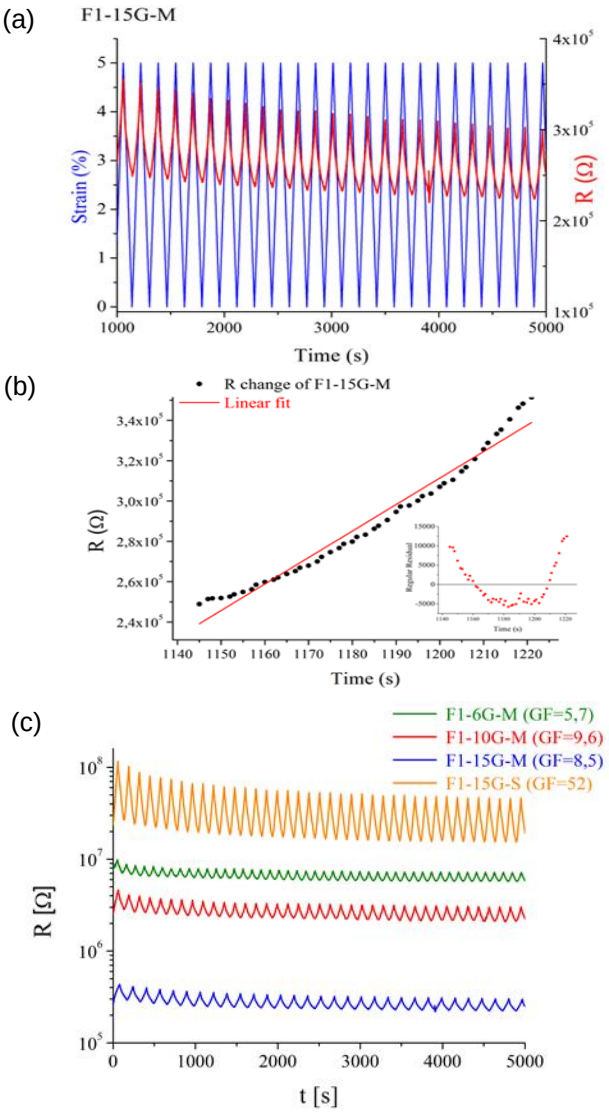

Fig. 6. Electromechanical behavior in terms of strain and relative resistance change for the F1-15G-M sample (a); example of R changes and relative straight line fitting of the F1-15G-M sample resistance (red line) (b); the residual of resistance R as a function of the time (in the insert of b); changing in resistance of the F1-6G-M, F1-10G-M, F1-15G-M, and F1-15G-S samples; GF are reported in the legend (c).

The not-linearity, assessed as the maximum percentage deviation of span of output value from the straight line, does not exceed by 4% for the F1-15G-M sample, calculated vs the mean value of the resistance change in the corresponding cycle (**Fig. 6b**). The maximum value of discrepancy between the linear fit and the resistance change was measured as 5% for the F1-6G-M sample.

Fig. 6c shows that in the M samples, the electrical resistance decreases as the graphene content increases, whereas the S sample shows the highest resistance. The huge difference in the resistance measured for the two samples F1-15G-M and F1-15G-S, can be attributed to two different factors. On the one hand, the higher porosity localized on the upper side of the F1-15G-M sample (see SEM images in **Fig. 2h**) can be responsible of the confinement of graphene platelets, which enhances the conductivity. On the other hand, the higher amount of isolated few-layers graphene nanoplateletes present in the F1-15G-S sample, and highlighted by the higher H_{1350}/H_{1575} ratio in **Fig. 5**, interrupts more likely the conductive pathway, reducing conductivity. Whereas the relatively poor dispersion of graphene in stirred samples facilitates the contacts among particles, and then the conductivity [**23**].

In this regards, in **Fig. 7**, the graphene platelets, which could be responsible of the conduction, are highlighted with red circles on the SEM images at 1000x of magnitude of the F1-15G-S (**Fig. 7a**) and F1-15G-M (**Fig. 7b**) samples, respectively. The schematic illustration show that a possible percolation path can be detected only for the F1-15G-M sample. Whereas for the F1-15G-S sample, there is always the coexistence of large aggregates and few-layer graphene platelets, but the latter are well dispersed, and the isolated platelets interrupt the electrical conduction.

Other authors [**25-28**] reported that homogeneous filler dispersion is important for mechanical properties while a good cluster distribution seems to be more significant for electrical properties [**28**].

Finally, the sensitivity of the piezoresistive strain sensors, expressed quantitatively as the gauge factor (GF):

$$GF = \frac{\Delta R / R}{\varepsilon}$$

where, ΔR/R is the normalized resistance and ε is the mechanical strain, was measured.

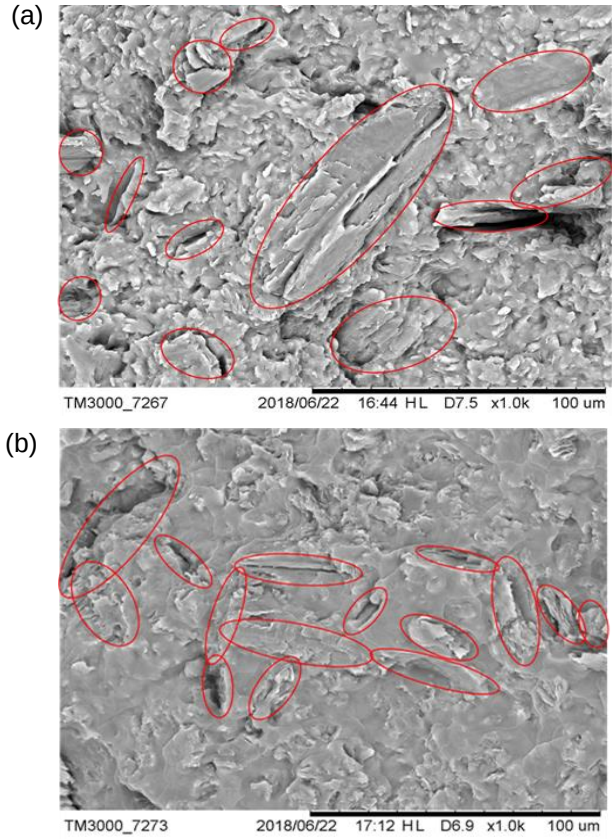

Fig. 7. Schematic illustration of the percolation in the F1-15G-S (a) and F1-15G-M (b) samples.

The GF for the M samples (see values in the legend of **Fig. 6**) increases as the graphene content increases; the S sample shows the highest value, i.e., 52, and then the highest sensitive. Again, the different behavior between sonicated and stirred samples might be ascribed to the different morphology of the samples and the dispersion degree of the graphene nanoplateletes. As previously discussed, the S samples shows the highest diffuse porosity, unlikely the M samples, which have porosity localized mostly in the upper side. The diffuse porosity allows the overall sample to be deformed during strain, improving the contact of nanoplateletes of graphene before distant, and then achieving the conductive pathways. In this way, the sonicated samples highlight a higher GF, in spite of the lower conductivity.

Conclusion

A low-viscosity elastomeric polymer was designed and prepared as matrix for the dispersion, by sonication or by stirring, of 6÷15wt% of graphene platelets, with the aim to manufacture highly stretchable strain sensors, capable to withstand in a wide range of temperature and high humidity. The low initial viscosity of the polymeric matrix was achieved by employing PDMS at low molecular weights. TEOS used as crosslinker contributes to further lower viscosity, and then to avoid the use of solvent for the filler's dispersion. In spite of the dispersion method, a strong adhesion between the graphene platelets and the polymeric matrix was found, and no detachment can be detected also at the highest concentration. As a consequence, the elastic modulus of the nanocomposites increases, and the elongation at break slightly decreases. Few-layer graphene platelets always coexist with large agglomerates, which concentration increases with the graphene content. The amount of the isolated few-layers graphene platelets is higher in the sonicated samples, which consequently exhibit a reduced conductivity. In fact, it was found that the relatively poor dispersion of graphene in stirred samples facilitates the contacts among particles, and then the conductivity. The porosity due to the evaporation of the developed solvents during the crosslinking reactions acts in a synergic way with the poor dispersion, confining the graphene nanoplateletes, and then achieving the conductivity of the stirred samples. The sensitivity of samples, measured as Gauge Factor, increases as the graphene content and the dispersion degree increase. All samples show quite no drift of the measured resistance in a wide range of operational conditions. Additionally, all nanocomposites exhibit a straight correspondence between the applied deformation and the measured resistance, since the non-linearity of the piezoresistive response is below the 5%.

Acknowledgements

This work was supported by the Italian Aerospace Research Centre (CIRA) internal funding, in the framework of the GRAphene-Polymeric Spray Sensor for shape recognition of super-deformable structures (GRAPSS) project. Authors also thank the National Research Council (CNR) since part of this work was realized in the framework of Joint Laboratory for Graphene-based Multifunctional Polymer Nanocomposites funded by CNR under the Joint Lab Call 2015–2018 Grant.

Author's contributions

Conceived the plan: FP; Performed the experiments: FP, GR, FS; Data analysis: FP, ML; Wrote the paper: FP, ML.

References

1. Balageas, D.; Fritzen, C.P.; Guemes, A., Structural Health Monitoring; John Wiley & Sons, **2010**, 496.
2. Zagrai, A.; Arritt, B.; Doyle, D., Structural Health Monitoring for Space Systems, Wiley, **2018**, 300.
3. Concilio, A.; Dimino, I.; Lecce, L.; Pecora, R., Morphing Wing Technologies: Large Commercial Aircraft and Civil Helicopters, Butterworth-Heinemann, **2017**, 978.
4. John Valasek, Morphing Aerospace Vehicles and Structures, John Wiley & Sons, **2012**, 312.
5. Concilio, A., Abstarct of paper, 24th AIAA/AHS Adaptive Structures Conference, AIAA SciTech, San Diego (CA-USA), **2016**.
6. Schorsch, O.; Lühring, A.; Nagel, C., Elastomer-Based Skin for Seamless Morphing of Adaptive Wings, in Smart Intelligent Aircraft Structures (SARISTU), Piet Christof Wölcken, Michael Papadopoulos (Eds.), 187, **2017**
7. Furlong, E.R., *J. Acoust. Soc. Am*., **2014**, *135*, 2275.
8. Tung, T. T., Nine, M. J., Krebsz, M., Pasinszki, T., Coghlan, C. J., Tran, D. N. H., & Losic, D., *Adv. Funct. Mater.*, **2017**, *27*, 1702891.
9. Zhan, Y.; Meng,Y.; Li, Y., *Materials Letters*, **2017**, 192, 115.
10. Zhao, J.; He, C.; Yang, R.; Shi, Z.; Cheng, M.; Yang, W.; Xie, G., *et al. Appl. Phys. Lett*., **2012**, *101*, 063112.
11. Yong, K.; Ashraf, A.; Kang, P.; Nam, S., *Sci. Rep*., **2016**, *6*, 24890.
12. Yan, C.; Wang, J.; Kang, Cui, M.; Wang, X.; Foo, C.Y., *et al. Adv. Mater*., **2014**, *26*, 2022.
13. Kim, K.S.; Zhao, Y.; Jang, H.; Lee, S.Y.; Kim, J.M.; Kim, K.S., *et al. Nature*, **2009**, *457*, 706.
14. Hempel, M.; Nezich, D.; Kong, J.; Hofmann, M., *Nano Lett.*, **2012**, *12*, 5714.
15. Bu, Q.; Zhan, Y.; He, F.; Lavorgna, M.; Xia, H., *J. Appl. Polym. Sci.* **2016**, *133*, 43243.
16. Scherillo, G., Lavorgna, M., Buonocore, G.G., Zhan, YH., Xia, H., Mensitieri, G., Ambrosio, L., *ACS Appl. Mater.Interfaces*, **2014**, *6*, 2230.
17. Yan, N., Buonocore, G., Lavorgna, M., Kaciulis, S., Balijepalli, S.K., Zhan, Y., Xia, H., Ambrosio, L., *Compos. Sci. Technol.*, **2014**, *102*, 74.
18. Wang, J., Zhang, K., Bu, Q., Lavorgna, M., Xia, H., Carbon-related Materials in Recognition of Nobel Lectures by Prof. Akira Suzuki in ICCE, **2017**, 175.
19. Wang, J., Zhang, K., Cheng, Z., Lavorgna, M., Xia, H., *Plast. Rubb. Compos*., **2018**, *47*, 398.
20. ISO Standard. Plastics—determination of tensile properties. Part 2. Test conditions for moulding and extrusion plastics. Reference ISO 527-2; **2002**(F).
21. Ni, Z.; Wang, Y.; Yu, T.; Shen, Z., *Nano Res*, **2008**, *1*, 273.
22. "Graphene" Synthesis, Properties and Phenomena, Ed. C.N.R. Rao and A.K. Sood, Wiley-VCH, **2013**, 307.
23. Kashi, S.; Gupta, R.K.; Baum, T.; Kao, N.; Bhattacharya, S.N., Materials and Design, **2016**, *109*, 68.
24. Li, J.; Kim, J.-K.; Lung Sham, M., *Scr. Mater.*, **2005**, *53*, 235;
25. Kim, H.; Kobayashi, S.; Abdur Rahim, M.A.; Zhang, M.J.; Khusainova, A.; Hillmyer, M.A.; Abdala, A.A.; Macosko, C.W., *Polymer*, **2011**, *52*, 1837.
26. Pan, Y.; Li, L.; Chan, S.H.; Zhao, J., *Compos. A: Appl. Sci. Manuf.*, **2010**, *41*, 419.
27. Aguilar, J.O.; Bautista-Quijano, J.R.; Aviles, F.; *Express Polym Lett*, **2010**, *4*, 292.
28. Cardoso, P.; Silva, J.; Klosterman, D.; Covas, J.A.; van Hattum, F.W. ; Simoes, R.; Lanceros-Mendez, S.; *Nanoscale Res. Lett*., **2011**, *6*, 370.

